Core photoionization of the argon dimer in the photon-energy range of 255–340 eV studied by a photoelectron-photoion-photoion coincidence technique

E. Keshavarz,[1] H. Farrokhpour,[2] H. Sabzyan,[1,*] Z. Noorisafa,[1] A. Kivimäki,[3] and R. Richter[4,*]

[1]*Department of Chemistry, University of Isfahan, Isfahan 81746-73441, Islamic Republic of Iran*

[2]*Department of Chemistry, Isfahan University of Technology, Isfahan 84156-83111, Islamic Republic of Iran*

[3]*Consiglio Nazionale delle Ricerche–Istituto Officina dei Materiali, Laboratorio TASC, 34149 Trieste, Italy*

[4]*Elettra-Sincrotrone Trieste, Area Science Park, 34149 Basovizza, Trieste, Italy*

(Received 9 March 2014; published 12 May 2014)

Single-photon multiple ionization of the argon dimer van der Waals complex, Ar_2, is studied by the photoelectron-photoion-photoion coincidence technique using synchrotron radiation in the photon-energy range of 255–340 eV, which covers the Ar $2p$ and Ar $2s$ ionization continua. Dissociation processes into $Ar^+ + Ar^+$, $Ar^+ + Ar^{2+}$, $Ar^+ + Ar^{3+}$, and $Ar^{2+} + Ar^{2+}$ ion pair channels are observed. The $Ar^+ + Ar^+$ and $Ar^+ + Ar^{2+}$ channels show the most intense ion-ion coincidences, compared to other observed dissociative channels. For the four observed channels the intensities are integrated and compared as functions of photon energy.

DOI: 10.1103/PhysRevA.89.053409 PACS number(s): 33.80.Eh, 33.15.Ta, 32.80.Hd

I. INTRODUCTION

The van der Waals interaction is very important in many areas of chemistry such as molecular scattering, chemical reaction precursor complexes, energy transfer intermediates, molecular recognition, protein folding, stacking of nucleobases, some types of self-assembly and supramolecular chemistry, solvation, condensation, and crystal packing [1–5]. From a fundamental point of view, the complexes formed by these noncovalent interactions are significant, as they bridge the gap between free molecular systems and the corresponding condensed phases [6]. Rare-gas van der Waals complexes have small dissociation energies ranging from ∼0.09 meV for He_2 [7] up to 12 meV for Ar_2 [8,9] resulting in large internuclear distances, such that they often behave as if each atom is nearly independent. These systems allow the investigation of a number of phenomena which emerge when an atom is embedded into an environment not observed for isolated atoms. Although the electronic ground states are very weakly bound, most rare-gas dimers support some vibrational levels with a shallow minimum [8–10]. The ions of the rare-gas dimers usually exhibit much deeper local minima in their potential energy surfaces and some of them present obvious chemical bonding characteristics [11–13]. The same holds for the doubly charged ions. For example, the well depth of the argon dimer dication, Ar_2^{2+}, is predicted to be 0.27 eV [14].

In recent years, in particular, the response to electronic excitation of atoms within small noble-gas clusters has been studied. In high-energy photoionization of light atoms, mainly ionization of inner-shell electrons occurs, and is usually followed by the Auger decay [15,16]. In clusters, the relaxation via electron emission can also result from energy or electron exchange between neighboring atomic sites, which was first predicted theoretically by Cederbaum *et al.* [17]. The competing decay mechanisms include interatomic Coulombic decay (ICD), electron transfer mediated decay (ETMD), and radiative charge transfer (RCT) [18,19]. Since fragmentation of the formed multiply charged ion occurs subsequently, various channels engaged in high-energy photoionization experiments can be disentangled using coincidence measurements [20–24].

Ionization experiments on argon dimers have been carried out using various techniques. The single ionization of Ar_2 by electron and photon impact has been investigated [24–28]. Imaging of the structure of the argon dimer and trimer has been carried out by measuring the momenta of all singly charged fragments in coincidence, following a double ionization process [29]. The double ionization potentials of argon clusters and the influence of the cluster size in the ionization process have been studied using the photoion-photoion coincidence (PIPICO) method [30,31]. Furthermore, the photoelectron-photoion-photoion coincidence (PEPIPICO) technique has been used to investigate the angular distribution of the photoelectron using photon energies of 252.0, 264.3, and 294.9 eV. No significant difference was found between the angular distributions of the Ar $2p$ photoelectrons of the argon monomer and dimer [32]. In addition, the mechanism of argon dimer multiple ionization and its following processes have received much attention from scientists in recent years. The ICD process in argon dimer ionization in the energy range of 32−77 eV has been investigated theoretically [33]. Lablanquie *et al.* have observed the ICD process after inner-valence ionization of Ar, Kr, and Xe dimers using synchrotron radiation [34]. Some papers have reported evidence of different decay mechanisms after core ionization or excitation of argon dimers by photons [35–40], which will be further discussed in the Results and Discussion section. Moreover, an ion impact ionization experiment has been carried out on argon dimers and the contribution of direct double ionization and RCT process in the production of $Ar^+ + Ar^+$ ion pair has been discussed [8,41]. Furthermore, following electron impact ionization (with electron energy of 120 eV), $Ar^+ + Ar^+$, $Ar^{2+} + Ar^+$, $Ar^{3+} + Ar^+$, and $Ar_2^+ + Ar^+$ ion pair channels have been observed and their production has been attributed to the ICD or RCT processes. Since the electron projectile energy (120 eV) was not sufficient to ionize core electrons, the whole ionization mechanism has been attributed to the valence or inner-valence ionization. Finally, another mechanism has been discussed in the context of the ion impact experiments, namely sequential

*Corresponding authors: sabzyan@sci.ui.ac.ir; robert.richter@elettra.edu

two-site ionization in which the two atomic centers are ionized subsequently by the projectile [42].

The double photoionization of a van der Waals complex has its own peculiarities. Such experiments on Ar_2 and ArNe complexes have recently been carried out at the Gas Phase Photoemission beamline of the Elettra synchrotron [40]. By scanning the synchrotron energy in the region of the Ar $2p_{3/2}^{-1}3d$, $2p_{3/2}^{-1}4d$, and $2p_{3/2}^{-1}5d$ resonances, the effect of the neighboring atom on the resonance energy has been revealed. Furthermore, the empirically predicted electron energy spectra (based on the experimental Auger spectra of the atom) at the three resonance energies have been compared to the experimental spectra, revealing that ICD is a major channel in the decay path following core excitation of the Ar_2 dimer.

In the present work, the single-photon multiple ionization of Ar_2 has been investigated by the PEPIPICO method in the energy range of 255−340 eV. Formation of the $Ar^+ + Ar^+$, $Ar^{2+} + Ar^+$, $Ar^{2+} + Ar^{2+}$, and $Ar^{3+} + Ar^+$ ion pairs observed after core ionization of the argon dimer in the entire energy range is discussed.

II. EXPERIMENT

The experiment is performed at the Gas Phase Photoemission beamline at the Elettra Synchrotron Laboratory. The beamline [43] and the end station [40] have already been described in detail elsewhere, so only a brief description of the experimental setup and conditions is presented here.

The experiment setup is shown schematically in Fig. 1. The setup used for the PEPIPICO experiment is a time-of-flight (TOF) apparatus with a 10.5-cm flight tube mounted along the polarization vector of the incident light at the end of the low-energy branch of the Gas Phase beamline.

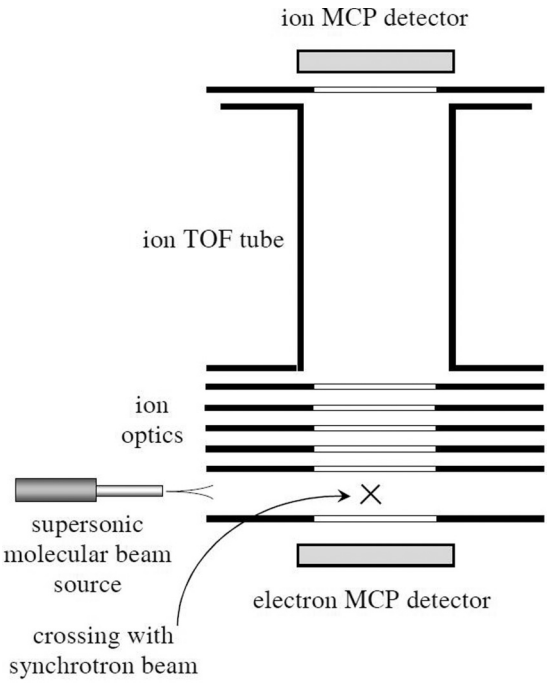

FIG. 1. A schematic diagram of the PEPIPICO experimental setup used in this study.

The cluster jet was created by supersonic expansion of Ar gas using a nozzle of 50 μm diameter, ∼15 mm distant from a skimmer of 500 μm diameter. The nozzle was cooled down to about −56 °C during the experiment. The stagnation pressure before the nozzle was about 1.3 bars while the ambient pressure in the ionization chamber was 3×10^{-6} mbar. Such conditions were set in order to maximize the yield of Ar_2 dimer formation, without producing many larger clusters. The mass spectra were recorded counting the ions signal as a function of the delay time, using electron pulses as the start signal. Both signals were fed into a multistop, 5-ns dead time, time-to-digital converter (TDC). Multiple ions produced in a short time window (6 μs) following the electron start pulse show up as ion-ion coincidences. The typical data accumulation period was between 1 and 2 h. The results presented here are not corrected for the detector efficiency, which is likely to favor the detection of more highly charged particles [44]. A computer was used to control all the components of the experiment and also to record data.

The time-of-flight spectra recorded at a photon energy of ∼20 eV and in the photon-energy range of 255–340 eV show a peak at $(m/q) = 80$, which indicates formation of the argon dimer, Ar_2^+. Especially at high photon energies, this ion is likely to be formed not only by the direct ionization of neutral dimers (Ar_2), but also by dissociative ionization of larger argon clusters which are inevitably present in the molecular beam. In the present analysis, we have therefore concentrated on ion-ion coincidence channels, where the application of momentum-matching conditions helps to identify the correlated decaying species.

The monochromatized synchrotron light beam entered the experimental setup horizontally, and crossed the beam containing atomic and molecular species, perpendicularly. The product ions were detected at a right angle, in coincidence with photoelectrons. A 1200 line/mm spherical grating (No. 4 among the five available gratings) set at the first diffraction order was used in the monochromator. The entrance and exit slits of the monochromator were adjusted in order to have a resolution of ∼30 meV in the investigated photon-energy range of 255–340 eV. The photon-energy scale calibration was checked by measuring the $2p$ and $2s$ excitations in the Ar atom.

III. RESULTS AND DISCUSSION

The corresponding initial states resulting from the ionization or excitation of the argon beam at selected photon energies have been listed in Table I. The events include Ar $2p$ or Ar $2s$ single-hole ionization, Ar $2p$ ionization accompanied by a valence electron excitation, and the Ar $2s \rightarrow np$ excitations. However, all these initial states decay further by a number of

TABLE I. Processes corresponding to the ionization excitation of Ar_2 dimer at selected photon energies.

Event	Threshold energy (eV)	Reference
Ionization to $2p_{3/2,1/2}^{-1}$	248.628, 250.776	[46]
Ionization to $2p^{-1}\ 3p^{-1}\ 4p$	∼270–275	[50]
Core excitation to $2s^{-1}4p$	323.6	[51]
Ionization to $2s^{-1}$	326.26	[52]

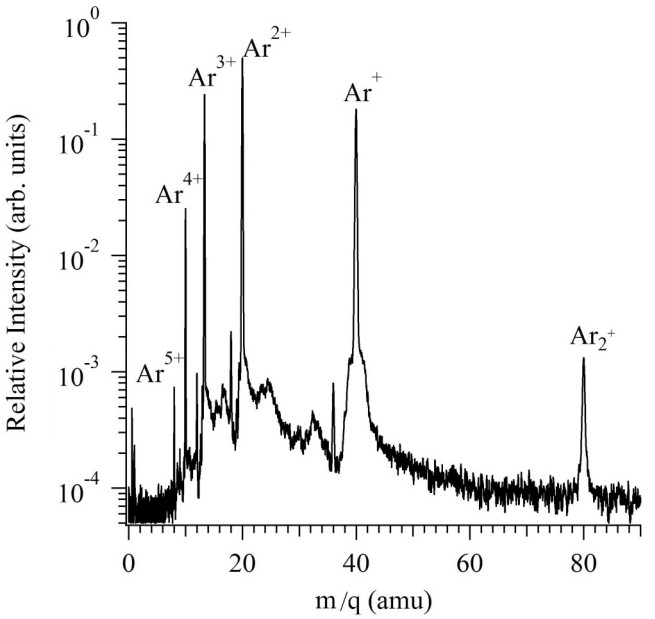

FIG. 2. An example of the mass spectrum recorded at the photon energy of 323.6 eV, near the maximum of the $2s \rightarrow 4p$ excitation. The main peaks are labeled on the graph.

mechanisms, including Auger decay, ICD, RCT, and ETMD, which will be discussed in more detail below.

An example of a mass spectrum recorded at the photon energy of 323.6 eV is presented in Fig. 2, with the corresponding ion-ion coincidence plot shown in Fig. 3(a). It should be mentioned that the coincidence plots recorded in the whole photon-energy range are very similar. The time-of-flight (TOF) spectrum shown in Fig. 2 contains all the detected electron-ion coincidence events. The TOF is therefore dominated by peaks due to the argon monomer. The kinetic energy content in the fragment ions produced by the dissociation of dimers or larger clusters causes a broadening of the peaks. This can be clearly observed, e.g., for the Ar^+ ion. The detection probability of an event depends on the collection efficiency for the electron and the corresponding ion. Simulations have shown that in our experimental setup electrons are collected with 100% efficiency up to a kinetic energy of ~120 eV. This efficiency drops to ~50% for a kinetic energy of 200 eV, which is the approximate energy of Auger electrons in the decay of Ar $2p$ hole states. Similarly, for Ar^+ ions 100% of particles with initial kinetic energies below 11 eV reach the detector.

The plot shown in Fig. 3(a) is the coincidence diagram between argon ions produced by Coulomb explosion of the Ar_2^{n+} in different ionization states n. The various regions of interest are marked on the graph. The highest intensity is observed for the $Ar^+ + Ar^+$ coincidence channel (region 1). By considering the momentum conservation law, for a species dissociating fast into two fragments A and B, the true coincidences should be located on a line with a slope of b given by [45]

$$b = \frac{p_B \cos\theta_B}{p_A \cos\theta_A}\left(\frac{q_A}{q_B}\right),$$

in which p_A and p_B are momenta of the A and B coincidence ions having q_A and q_B charges, and θ_A and θ_B are the angles describing trajectories of the two ions with respect to the detector

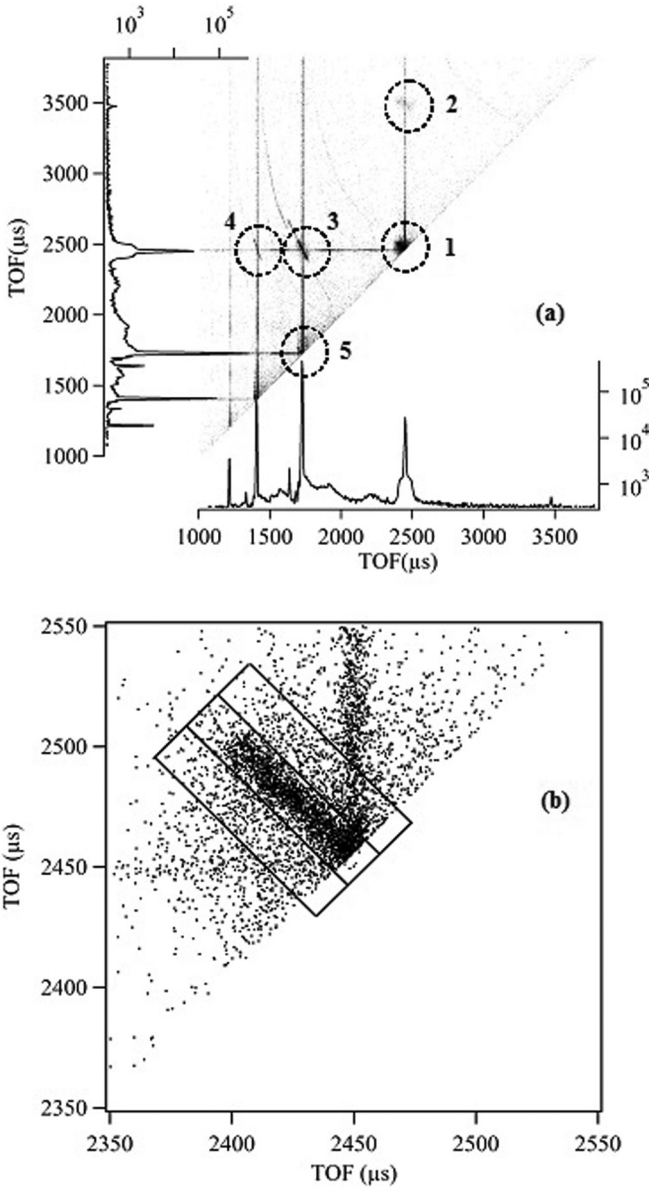

FIG. 3. (a) The ion-ion time-of-flight correlation diagram corresponding to the $Ar^+ + Ar^+$ (region 1), $Ar^{2+} + Ar^+$ (region 3), and $Ar^{3+} + Ar^+$ (region 4) coincidences. The weak $Ar_2^+ + Ar^+$ (region 2) and $Ar^{2+} + Ar^{2+}$ (region 5) coincidence traces can also be observed. (b) The partitioning scheme used for the integration of the coincidence signals and background correction, depicted for region 1.

direction, respectively. Since in a Coulomb explosion process, the two ions would be released in the opposite directions, we have $\cos\theta_A = -\cos\theta_B$. For the $Ar^+ + Ar^+$ coincidences, this slope is $b = -1$. The coincidences surrounding this area can be attributed to the random coincidences that are present all over the spectrum, or to the coincidences between the Ar^+ ions produced from dissociation of larger argon clusters. The explosion of larger clusters follows the momentum conservation law, but their coincidence tracks would not be located on the same line as that of the $Ar^+ + Ar^+$ coincidence from the Ar_2^{2+} fragmentation. An evidence of the formation of larger clusters is the weak coincidence between Ar^+ and Ar_2^+ ions (region 2), as the result of the fragmentation of $Ar_{n\geqslant 3}^{2+}$ cluster.

In Fig. 3, the $Ar^{2+} + Ar^{+}$ coincidence (region 3) can be observed with a slope of -2, which has less intensity than that of the $Ar^{+} + Ar^{+}$ coincidence line. The $Ar^{3+} + Ar^{+}$ coincidence (region 4) can also be seen, with a slope of -3, with the least intensity in this series. The $Ar^{2+} + Ar^{2+}$ coincidence can also be traced (region 5), with a slope of -1, but with low counts overlapped by false coincidences, making its analysis difficult. At the highest photon energy used in the present experiment a very weak signal due to $Ar^{2+} + Ar^{3+}$ events is observed, but due to its low statistics it is impossible to quantify it. In addition, the ion coincidence plot shows some weak diagonal traces of false, spurious coincidences, dissociation of larger clusters, and signals due to background gas in the chamber.

The coincidence yields of the various channels are extracted from the data by counting the number of ion-ion coincidence events in the appropriate regions of the plot, making use of the momentum-matching condition along the spectrometer axis. In order to estimate the contribution of the false coincidences, events in the neighboring sections were also evaluated, averaged, and subtracted [Fig. 3(b)] from the signal in the region of interest. While this procedure is relatively straightforward when evaluating signals due to ions of different m/q, it is more difficult for events originating from two identical ions [e.g., region 1 in Fig. 3(a)]. In a one-dimensional single-detector TOF spectrometer, the detection of such events occurring almost simultaneously is limited by the combined dead time of the detector and electronics. Events occurring during this dead time ($\sim$5 ns in this experiment) are not counted. While their contribution can be estimated making some assumptions about the angular distribution of the ions, this increases the error, especially if the yield of a particular channel is low. In order to estimate this correction, we have assumed that the $Ar^{+} + Ar^{+}$ and $Ar^{2+} + Ar^{2+}$ channels are isotropic. The dead time of the detector is the main reason for the large error in the determination of the $Ar^{2+} + Ar^{2+}$ coincidence yield at all photon energies (Fig. 4).

The ion-ion coincidence data are also used to estimate the kinetic energy release (KER) into the fragments for three of the four detected decay channels. In our experimental setup, only the projection of the initial velocity vector of the ions on the spectrometer axis can be extracted from the arrival times. We applied this analysis to the arrival time profiles of the Ar^{+} ions detected in coincidence with Ar^{+}, Ar^{2+}, and Ar^{3+} partners. For the three channels we obtain a KER of $\sim$4.5, $\sim$6, and $\sim$7.8 eV, respectively. The contributions of various decay processes generating the same final ionic charge cannot be separated, as the kinetic energy of the electrons emitted in the process is not analyzed. Within the accuracy of our experiment, the KER remains unchanged at the selected photon energies. For comparison, the energy of the fragments produced at the ground state's equilibrium distance of the neutral dimer ($\sim$3.8 Å [9]) is 3.8, 7.6, and 11.3 eV for the channels $Ar^{+} + Ar^{+}$, $Ar^{+} + Ar^{2+}$, and $Ar^{+} + Ar^{3+}$, respectively. We note that for the first channel, the experimentally determined KER is larger than that observed for a Coulomb explosion at the ground-state geometry, indicating that the dissociation proceeds via a more tightly bound higher-lying state(s) of the doubly charged complex. This has been studied in detail above the Ar $2p$ threshold in experiments where determination

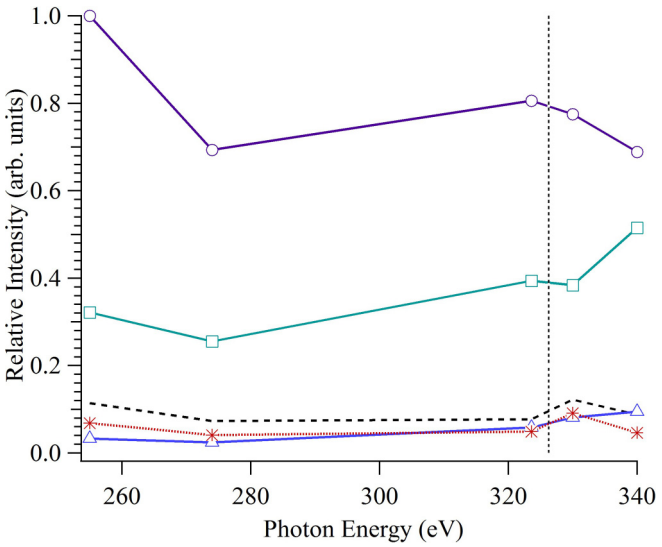

FIG. 4. (Color online) The normalized yields of the $Ar^{+} + Ar^{+}$ (circles), $Ar^{2+} + Ar^{+}$ (squares), $Ar^{3+} + Ar^{+}$ (triangles), and $Ar^{2+} + Ar^{2+}$ (stars) coincidence channels shown as functions of photon energy. Each line connects the data points corresponding to a single selected energy. For the $Ar^{2+} + Ar^{2+}$ channel, an upper error limit determined in the analysis is also indicated (dashed line). The data are not corrected for the detector response. The Ar $2s$ ionization threshold is indicated by the dotted vertical line.

of the kinetic energy of the corresponding electrons permitted separation of the various decay channels [32,35,36].

The initial processes corresponding to the selected photon energies are listed in Table I, and the major relevant decay processes are shown in Fig. 5. At the photon energy of 255 eV, only Ar $2p$ single-hole ionization is possible (neglecting valence photoionization channels) [46]. Near this photon energy, the photoionization of argon dimer has been investigated in much detail experimentally [32,35,36] and theoretically [33]. The basic decay mode is Auger decay, which produces Ar^{2+} states. It means that in dimers, the two holes are located originally in the same Ar atom. It has been shown in previous studies that they may be separated by RCT process to produce $Ar^{+} + Ar^{+}$ coincidences [35]. Some final states of Auger decay can decay further by ICD [33,36], which results in $Ar^{+} + Ar^{2+}$ coincidences. The Ar $2p^{-1}$ states can also undergo direct or cascade double Auger decay, which happens with a probability of about 13%$-$20% in Ar atoms [47–49]. The Ar^{3+} final states of $3s^{-1}\,3p^{-2}$ and $3p^{-3}$ configurations have also been observed. The double Auger decay may take place with similar probability in Ar dimers, which then results in $Ar - Ar^{3+}$ pairs. While the $3p^{-3}$ states are located at lower energy, for some $3s^{-1}3p^{-2}$ states decays via ETMD and ICD processes have been observed, which result in $Ar^{2+} + Ar^{2+}$ and $Ar^{+} + Ar^{3+}$ coincidences, respectively [37]. Experimentally, the $Ar^{+} + Ar^{3+}$ coincidence channel has not been reported previously at this photon energy.

At higher energies, the $2p$ ionization of Ar is still expected to be the dominating process, as its cross section remains high. Going to the photon energy of 270–275 eV, shake-up processes become possible in the context of Ar $2p$ ionization, yielding, for instance, the Ar $2p^{-1}3p^{-1}np$ satellite states [50],

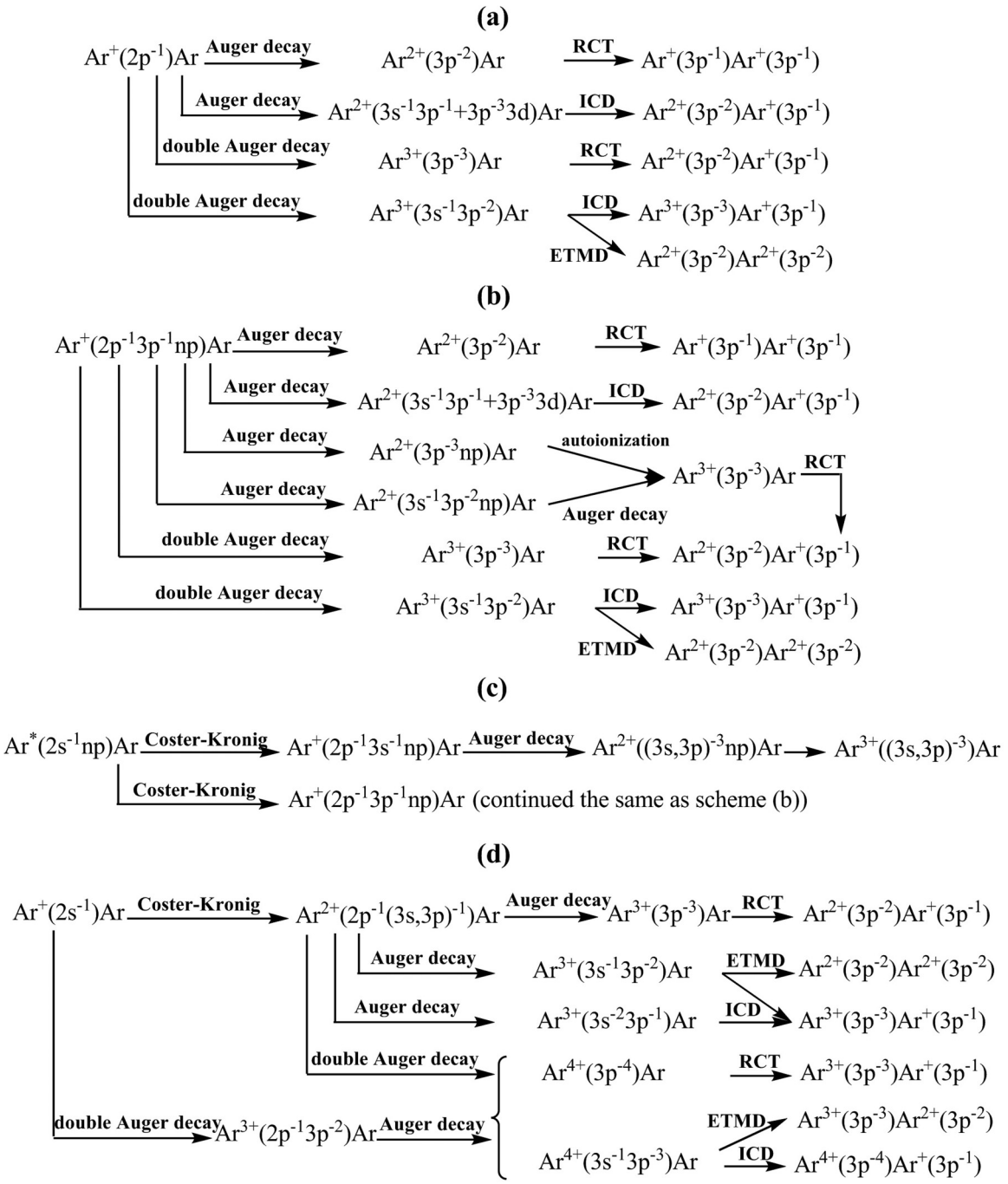

FIG. 5. Major decay processes following the initial ionization or excitation process at photon energies of (a) 255, (b) 274, (c) 325, and (d) 330 and 340 eV. For brevity, final fragmentation products are not mentioned in (c), because this state turns into similar intermediate states as given for (b).

although its relative cross section is low. Taking the $4p$ state as an example, the $4p$ electron likely acts as a spectator in the first-step Auger decay, which would then gives final states of $3p^{-3}4p$, $3s^{-1}3p^{-2}4p$, and $3s^{-2}3p^{-1}4p$ configurations, with the first states dominating the spectra [49]. Many of these states are located in the energy range just below the Ar triple ionization potential. Thus for some $\mathrm{Ar} - \mathrm{Ar}^{2+}$ first-step Auger states, a second-step Auger decay may not be possible, but ICD and RCT are possible, which may contribute to the $\mathrm{Ar}^{+} + \mathrm{Ar}^{2+}$ and $\mathrm{Ar}^{+} + \mathrm{Ar}^{+}$ coincidence yield [35,36]. For other states, the electron in the $4p$ orbital increases the probability that these final states decay further in a second-step Auger decay, as compared to that of the $2p$ single-hole ionization [49]. The increased probability of Ar^{3+} production can be translated to an increased yield of the $\mathrm{Ar}^{2+} + \mathrm{Ar}^{2+}$ and $\mathrm{Ar}^{+} + \mathrm{Ar}^{3+}$ channels.

The $2s \rightarrow 4p$ excitation occurs around the photon energy of 323.6 eV [51], which has not so far been investigated in the argon dimer. The Ar $2s^{-1}4p^{1}$ core-excited states mostly decay via transitions $2s^{-1}4p^{1} \rightarrow 2p^{-1}3s^{-1}4p^{1}$ and $2s^{-1}4p^{1} \rightarrow$

$2p^{-1}3p^{-1}4p^{1}$, i.e., through resonant Coster-Kronig decay [51]. In both of these final states, the $2p$ hole can decay further via second-step Auger decay, increasing the charge state to +2 and reaching final states such as $3s^{-2}3p^{-1}4p$, $3s^{-1}3p^{-2}4p$, and $3p^{-3}4p$ [49]. These final states are actually the same as that obtained after Ar $2p$ shake-up ionization, considered above.

Finally, creation of a $2s$ hole [52] above the photon energy of 326.3 eV leads to Coster-Kronig transitions $2s^{-1} \rightarrow 2p^{-1}3s^{-1}$ and $2s^{-1} \rightarrow 2p^{-1}3p^{-1}$. As discussed above, the Ar $2p$ hole is filled in the second-step Auger decay, resulting in triply charged Ar [48]. The next probable step may be RCT, ICD, or ETMD which gives $Ar^{+} + Ar^{2+}$, $Ar^{+} + Ar^{3+}$, and $Ar^{2+} + Ar^{2+}$ coincidences, respectively [35,37]. If double Auger takes place in either decay step (when filling the $2s$ hole and subsequently the $2p$ hole), one could expect many $Ar - Ar^{4+}$ complexes after decay. The possibility for such cascade in the argon atom is 10% [48]. The $Ar - Ar^{4+}$ complex can undergo further decays with the possibility of observing $Ar^{+} + Ar^{3+}$ and more highly charged coincidences, like $Ar^{3+} + Ar^{2+}$ or $Ar^{+} + Ar^{4+}$.

Figure 4 shows the normalized integrated intensities of the different coincidence yields, corrected for false coincidences, as functions of photon energy. The data have been internally normalized by setting the $Ar^{+} + Ar^{+}$ channel intensity at 255 eV to 1. This channel slowly decreases with increasing energy in the investigated energy range, while still remaining by far the most intense over the whole energy range. This may reflect the decrease in the Ar $2p$ photoionization cross section. For the $2s$ ionization region, the branching ratio towards all more highly charged species, in particular of $Ar^{+} + Ar^{3+}$ and $Ar^{2+} + Ar^{2+}$, has been increased. As discussed above, after the $2s$ hole creation, the probability for triply charged argon production is high (it is ~89% for atomic Ar $2s^{-1}$, compared to ~13% for atomic Ar $2p^{-1}$ [48]), and thus, the contribution of the resulting channels would be higher, in comparison with that at other photon energies.

IV. CONCLUSION

The multiple photoionization of Ar_2 dimer in the photon-energy range of 255−340 eV has been studied by the use of synchrotron light source and the PEPIPICO technique. The analysis of the PEPIPICO diagrams shows that, for the whole energy range, dissociative ionization produces $Ar^{+} + Ar^{+}$, $Ar^{+} + Ar^{2+}$, $Ar^{+} + Ar^{3+}$, and $Ar^{2+} + Ar^{2+}$ ion pairs. The contribution of more highly charged states increases with increasing photon energy. Without analysis of the kinetic energy of the emitted electrons, a detailed interpretation of the decay processes is not possible based on the experimental data only. By analysis of the results of previous studies [32,33,36,37], the observed decay channels are rationalized by comparing with those of the argon atom.

ACKNOWLEDGMENTS

We thank the staff of the Gas Phase beamline and all our colleagues at Elettra for their support during the experiments. E.K., H.F., H.S., and Z.N. would like to express thanks for the support from University of Isfahan and Isfahan University of Technology. E.K., H.F., and H.S. are grateful to the ICTP for financial support under the ICTP-Elettra users program.

[1] K. Müller-Dethlefs and P. Hobza, Chem. Rev. **100**, 143 (2000).
[2] Y. Zhao and D. G. Truhlar, J. Phys. Chem. A **110**, 5121 (2006).
[3] J. F. Dobson, K. McLennan, A. Rubio, J. Wang, T. Gould, H. M. Le, and B. P. Dinte, Aust. J. Chem. **54**, 513 (2001).
[4] A. Ruzsinszky, J. P. Perdew, and G. L. Csonka, J. Phys. Chem. A **109**, 11015 (2005).
[5] J. A. Dobado and J. Molina, J. Phys. Chem. A **103**, 4755 (1999).
[6] D. Bressanini and G. Morosi, J. Phys. Chem. A **115**, 10880 (2011).
[7] R. E. Grisenti, W. Schöllkopf, J. P. Toennies, G. C. Hegerfeldt, T. Köhler, and M. Stoll, Phys. Rev. Lett. **85**, 2284 (2000).
[8] T. V. Mourik, A. K. Wilson, and T. H. Dunning, Jr., Mol. Phys. **96**, 529 (1999).
[9] S. M. Cybulski and R. R. Toczyłowski, J. Chem. Phys. **111**, 10520 (1999).
[10] B. Jäger, R. Hellmann, E. Bich, and E. Vogel, Mol. Phys. **107**, 2181 (2009).
[11] J. S. Cohen and B. Schneider, J. Chem. Phys. **61**, 3230 (1974).
[12] F. X. Gadea and I. Paidarová, Chem. Phys. **209**, 281 (1996).
[13] I. Paidarová and F. X. Gadea, Chem. Phys. **274**, 1 (2001).
[14] J. Ackermann and H. Hogreve, Chem. Phys. Lett. **202**, 23 (1993).
[15] N. Saito and I. H. Suzuki, Int. J. Mass. Spectrom. Ion Procces. **115**, 157 (1992).
[16] P. Lablanquie, F. Penent, R. I. Hall, H. Kjeldsen, J. H. D. Eland, A. Muehleisen, P. Pelicon, Ž. Šmit, M. Žitnik, and F. Koike, Phys. Rev. Lett. **84**, 47 (2000).
[17] L. S. Cederbaum, J. Zobeley, and F. Tarantelli, Phys. Rev. Lett. **79**, 4778 (1997).
[18] J. Zobeley, R. Santra, and L. S. Cederbaum, J. Chem. Phys. **115**, 5076 (2001).
[19] K. Kreidi, T. Jahnke, T. Weber, T. Havermeier, X. Liu, Y. Morisita, S. Schössler, L. P. H. Schmidt, M. Schöffler, M. Odenweller, N. Neumann, L. Foucar, J. Titze, B. Ulrich, F. Sturm, C. Stuck, R. Wallauer, S. Voss, I. Lauter, H. K. Kim *et al.*, Phys. Rev. A **78**, 043422 (2008).
[20] B. Ulrich, A. Vredenborg, A. Malakzadeh, M. Meckel, K. Cole, M. Smolarski, Z. Chang, T. Jahnke, and R. Dörner, Phys. Rev. A **82**, 013412 (2010).
[21] B. Manschwetus, H. Rottke, G. Steinmeyer, L. Foucar, A. Czasch, H. Schmidt-Böcking, and W. Sandner, Phys. Rev. A **82**, 013413 (2010).
[22] T. Jahnke, A. Czasch, M. S. Schöffler, S. Schössler, A. Knapp, M. Käsz, J. Titze, C. Wimmer, K. Kreidi, R. E. Grisenti, A. Staudte, O. Jagutzki, U. Hergenhahn, H. Schmidt-Böcking, and R. Dörner, Phys. Rev. Lett. **93**, 163401 (2004).
[23] T. Aoto, K. Ito, Y. Hikosaka, E. Shigemasa, F. Penent, and P. Lablanquie, Phys. Rev. Lett. **97**, 243401 (2006).

[24] K.-M. Weitzel, M. Penno, J. Mähnert, and H. Baumgärtel, Z. Phys. D **29**, 195 (1994).
[25] H. Helm, K. Stephan, and T. D. Märk, Phys. Rev. A **19**, 2154 (1979).
[26] T. Pflüger, A. Senftleben, X. Ren, A. Dorn, and J. Ullrich, Phys. Rev. Lett. **107**, 223201 (2011).
[27] P. M. Dehmer and J. L. Dehmer, J. Chem. Phys. **69**, 125 (1978).
[28] T. Pradeep, B. Niu, and D. A. Shirley, J. Chem. Phys. **98**, 5269 (1993).
[29] B. Ulrich, A. Vredenborg, A. Malakzadeh, L. Ph. H. Schmidt, T. Havermeier, M. Meckel, K. Cole, M. Smolarski, Z. Chang, T. Jahnke, and R. Dörner, J. Phys. Chem. A **115**, 6936 (2011).
[30] E. Rühl, C. Schmale, H. C. Schmelz, and H. Baumgärtel, Chem. Phys. Lett. **191**, 430 (1992).
[31] E. Rühl, C. Schmale, H. W. Jochims, E. Biller, M. Simon, and H. Baumgärtel, J. Chem. Phys. **95**, 6544 (1991).
[32] A. De Fanis, M. Oura, N. Saito, M. Machida, M. Nagoshi, A. Knapp, J. Nickles, A. Czasch, R. Dörner, Y. Tamenori, H. Chiba, M. Takahashi, J. H. D. Eland, and K. Ueda, J. Phys. B: At. Mol. Opt. Phys. **37**, L235 (2004).
[33] S. D. Stoychev, A. I. Kuleff, F. Tarantelli, and L. S. Cederbaum, J. Chem. Phys. **128**, 014307 (2008).
[34] P. Lablanquie, T. Aoto, Y. Hikosaka, Y. Morioka, F. Penent, and K. Ito, J. Chem. Phys. **127**, 154323 (2007).
[35] N. Saito, Y. Morishita, I. H. Suzuki, S. D. Stoychev, A. I. Kuleff, L. S. Cederbaum, X.-J. Liu, H. Fukuzawa, G. Prümper, and K. Ueda, Chem. Phys. Lett. **441**, 16 (2007).
[36] Y. Morishita, X.-J. Liu, N. Saito, T. Lischke, M. Kato, G. Prümper, M. Oura, H. Yamaoka, Y. Tamenori, I. H. Suzuki, and K. Ueda, Phys. Rev. Lett. **96**, 243402 (2006).
[37] K. Sakai, S. Stoychev, T. Ouchi, I. Higuchi, M. Schöffler, T. Mazza, H. Fukuzawa, K. Nagaya, M. Yao, Y. Tamenori, A. I. Kuleff, N. Saito, and K. Ueda, Phys. Rev. Lett. **106**, 033401 (2011).
[38] M. Kimura, H. Fukuzawa, K. Sakai, S. Mondal, E. Kukk, Y. Kono, S. Nagaoka, Y. Tamenori, N. Saito, and K. Ueda, Phys. Rev. A **87**, 043414 (2013).
[39] M. Kimura, H. Fukuzawa, T. Tachibana, Y. Ito, S. Mondal, M. Schoffler, J. Williams, Y. Jiang, N. Saito, and K. Ueda, J. Phys. Chem. Lett. **4**, 1838 (2013).
[40] P. O'Keeffe, E. Ripani, P. Bolognesi, M. Coreno, M. Devetta, C. Callegari, M. Di Fraia, K. C. Prince, R. Richter, M. Alagia, A. Kivimäki, and L. Avaldi, J. Phys. Chem. Lett. **4**, 1797 (2013).
[41] J. Matsumoto, A. Leredde, X. Flechard, K. Hayakawa, H. Shiromaru, J. Rangama, C. L. Zhou, S. Guillous, D. Hennecart, T. Muranaka, A. Mery, B. Gervais, and A. Cassimi, Phys. Scr. **T144**, 014016 (2011).
[42] T. Pflüger, Ph.D. thesis, University of Heidelberg, 2012.
[43] R. R. Blyth, R. Delaunay, M. Zitnik, J. Krempasky, R. Krempaska, J. Slezak, K. C. Prince, R. Richter, M. Vondracek, R. Camilloni, L. Avaldi, M. Coreno, G. Stefani, C. Furlani, M. de Simone, S. Stranges, and M.-Y. Adam, J. Electron Spectrosc. Relat. Phenom. **101–103**, 959 (1999).
[44] M. Krems, J. Zirbel, M. Thomason, and R. D. DuBois, Rev. Sci. Instrum. **76**, 093305 (2005).
[45] S.-J. King, Ph.D. thesis, University College London, 2008.
[46] L. Avaldi, G. Dawber, R. Camilloni, G. C. King, M. Roper, M. R. F. Siggel, G. Stefani, and M. Zitnik, J. Phys. B: At. Mol. Opt. Phys. **27**, 3953 (1994).
[47] J. Viefhaus, S. Cvejanović, B. Langer, T. Lischke, G. Prümper, D. Rolles, A. V. Golovin, A. N. Grum-Grzhimailo, N. M. Kabachnik, and U. Becker, Phys. Rev. Lett. **92**, 083001 (2004).
[48] S. Brünken, C. Gerth, B. Kanngießer, T. Luhmann, M. Richter, and P. Zimmermann, Phys. Rev. A **65**, 042708 (2002).
[49] M. Nakano, Y. Hikosaka, P. Lablanquie, F. Penent, S.-M. Huttula, I. H. Suzuki, K. Soejima, N. Kouchi, and K. Ito, Phys. Rev. A **85**, 043405 (2012).
[50] G. C. King, M. Tronc, F. H. Read, and R. C. Bradford, J. Phys. B: At. Mol. Phys. **10**, 2479 (1977).
[51] R. Sankari, A. Kivimäki, M. Huttula, T. Matila, H. Aksela, S. Aksela, M. Coreno, G. Turri, R. Camilloni, M. de Simone, and K. C. Prince, Phys. Rev. A **65**, 042702 (2002).
[52] P. Glans, R. E. LaVilla, M. Ohno, S. Svensson, G. Bray, N. Wassdahl, and J. Nordgren, Phys. Rev. A **47**, 1539 (1993).